CERAMIC AND HYBRID MICRO-ARCHITECTED MATERIALS FOR HIGH TEMPERATURE APPLICATIONS

Andrew L. R. Moodie[1], Jesse P. Angle[2], Edward C. Tackett[3], Timothy J. Rupert[1,2], Martha L. Mecartney[2], Lorenzo Valdevit[1,2]

[1]Mechanical and Aerospace Engineering Department, University of California, Irvine

[2]Chemical Engineering and Materials Science Department, University of California, Irvine

[3]RapidTech, NSF DUE 1104305, University of California, Irvine

Irvine, CA 92697

ABSTRACT

This article presents an innovative additive manufacturing approach for fully optimized ceramic and hybrid (ceramic/polymer) hierarchical micro-architected materials for extreme environments. The developed materials combine high-temperature capabilities, extremely low thermal conductivity, high stiffness and strength per unit weight, sufficient toughness and great resistance to oxidation. Processing involves 3D printing of a ceramic architecture, followed by bisque firing and sintering. When sufficient porosity remains after sintering (~50%), infiltration by a polymeric matrix is possible, resulting in a cellular architecture where the constituent material is a fully dense ceramic/polymer hybrid with exceptional ductility. After characterizing the microstructure and mechanical properties of the constituent material (ceramic and hybrid), we demonstrate the fabrication of a truss-core sandwich panel. Both the internal architecture and the external shape can be controlled at will in the manufacturing process. Multifunctional Thermal Protection Systems (TPS) for the next generation of high-speed aircraft (particularly hypersonics) are the prototypical, albeit not the only, application.

1. INTRODUCTION

The development of ever faster air vehicles requires the introduction of novel Thermal Protection Systems (TPS), to contend with increasing thermal loads on leading edges, acreage and combustor walls[1]. Current TPS (e.g., Space Shuttle tiles) are structurally parasitic, and significant weight saving is expected with a multi-functional (thermo-structural) design. Metallic sandwich structures with topologically architected cellular cores have been extensively analyzed for thermo-structural benefits over the past decade [2]-[5], including for applications to actively cooled hypersonic combustor walls [6]-[9]. The challenge in transferring these design concepts to passive TPS for hypersonic vehicles is related to materials and processes development: ceramic outer skins and cores are necessary to withstand the enormous temperatures (often in excess of 1,500C); additionally, often the internal face sheet must be compatible with Carbon-epoxy or Carbon-polyimide composites (PMCs). Traditional manufacturing of architected

ceramic components is particularly challenging, given the difficulty in machining and/or bonding ceramic materials.

This work explores the applicability of novel (but commercially available) *digital additive manufacturing technologies* (in particular 3D printing) with *architecture design approaches* to demonstrate and characterize ceramic and hybrid (ceramic/polymer) sandwich structures with architected cores for optimal combinations of *high stiffness, high strength, low thermal conductivity and low weight.* The proposed multifunctional TPS sandwich structure is depicted in Fig. 1: the fully ceramic version (a) comprises two ceramic matrix composite (or ceramic) face sheets and a ceramic micro-architected core; the hybrid version (b) uses polymer matrix composites (PMC) for the internal face sheet, mechanically bonded to the ceramic core.

The manufacturing approach involves 3D printing of the desired ceramic architecture (possibly including the face sheets), followed by either densification upon sintering or partial sintering followed by polymer infiltration in the residual porosity. This manufacturing technique allows a high level of design flexibility, resulting in potentially complex architectures that are impossible or impractical to manufacture with any other approach (e.g., cast forming or machining).

This work demonstrates 3D printing of fully ceramic truss-core sandwich panels with interconnected porosity at the material (i.e. at the truss member) level, and the subsequent full infiltration of that porosity with a slow curing epoxy resin. The microstructure and the mechanical properties of the constituent material (alumina (Al_2O_3) / mullite ($3Al_2O_3 \cdot 2SiO_2$) /epoxy hybrid) are characterized, and the performance of the infiltrated panel under compressive loads is discussed.

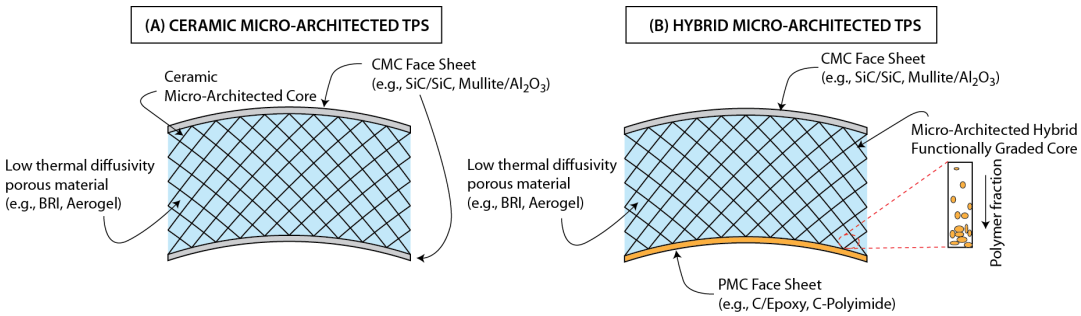

Figure 1. Schematic of a multifunctional Thermal Protection Systems (TPS) concept. (A) Fully Ceramic; (B) Functionally graded hybrid (ceramic/polymer).

2. EXPERIMENTATION

2.1 Fabrication of ceramic and hybrid architected materials

2.1.1 3D printing of alumina/silica ceramics

All ceramics described in this work were processed by 3D printing, using a Zprinter 310. The printing procedure can be summarized as follows: 100µm-thick layers of dry alumina/silica (Al_2O_3 / SiO_2) powder (Virishell, from Viridis3D, LLC) are sequentially deposited, and an inkjet system is used to print a liquid binder on selected areas of each layer, according to a .SLS file generated by a CAD application. Upon removal from the printer, the part is placed in a drying oven, and subsequently dusted to remove residual dry powder. To increase bonding between the

particles, the part is submerged in tetraethylorthosilicate (TEOS), which is solidified in the presence of ammonia vapor at room temperature to form a thin layer of silica. Prior to sintering, the dried printed samples were bisque fired at 1200°C for 10 hours to slowly burn off excess organic binder used in the printing process. Pressure-less sintering of bisque fired samples was performed in air at 1550°C for 3 hours. A constant ramp rate of 10°C/min was used for both the heat up and cool down steps. Samples which appeared discolored after sintering due to insufficient binder burn-off were rejected and discarded. The shrinking resulting from sintering was essentially isotropic, with no major effect on the architecture of the part.
This process resulted in samples approximately 50% dense (see Sec. 3.2), but much higher density can be obtained by fine-tuning the powder composition, initial powder particle size, the binder chemistry and the sintering parameters. An example of an architected ceramic sandwich panel is depicted in Fig. 2.

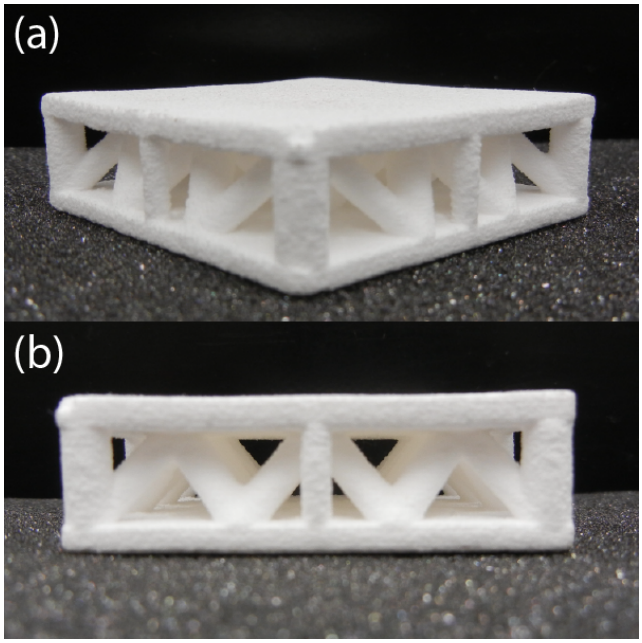

Figure 2 – 3D printed alumina/silica architected sandwich panel after bisque firing and sintering. (a) Isometric view; (b) Front view. The external vertical columns were printed to support the face sheet during sintering and preserve the shape of the part. They were removed prior to infiltration and testing.

2.1.2 Fabrication of functionally graded ceramic/polymer hybrids

Due to the relatively large particle size of the alumina/silica powder (sec. 3.1), the constituent material of the sintered ceramic structure is porous enough to provide infiltration by capillary action when partially submerged into a liquid. By using a slow-setting polymer, the infiltration depth into the ceramic can be controlled, potentially resulting in a functionally graded material transitioning from a porous ceramic to a fully dense ceramic/polymer hybrid over a desired length. Figure 3a exemplifies the process. A sintered printed ceramic cylinder was set in slow curing epoxy on one end. The epoxy wicked though portion of the material, flowing against gravity by capillary action. Food coloring was used to track the hybrid/ceramic interface (Fig. 3b). Fig. 3c display the distribution of porosity on the cross-section of Fig. 3b (obtained by

image manipulation). The absence of porosity (black) on the bottom portion of the sample indicates near-full infiltration by the polymer. As the extension of wicking is a function of the porosity size and morphology in the sintered ceramic, it can be tailored by controlling the ceramic powder particle size and distribution, the binder chemistry and the sintering schedule.

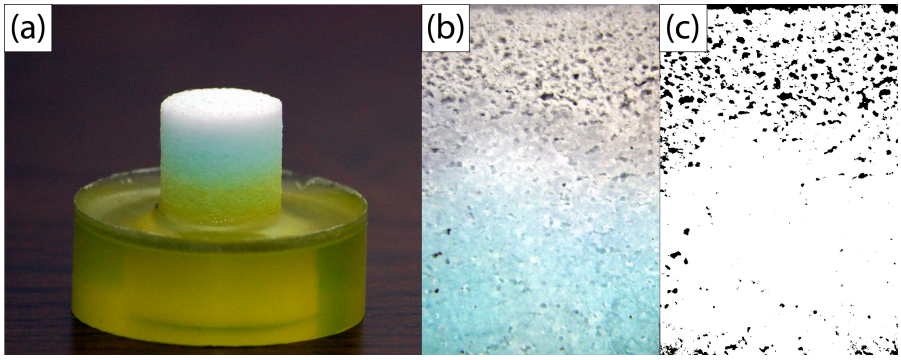

Figure 3 – (a) Sintered ceramic cylinder embedded in epoxy resin. Notice that the resin partially wicks through the cylinder (coloring was added to emphasize the gradient in composition). (b) Optical micrograph of a cross-section of the cylinder in (a), showing a gradient in resin volume fraction; (c) Digital thresholding of the image in (b), clearly showing a gradient in porosity. Notice that the infiltrated (hybrid) regions are nearly fully dense, whereas ~50% porosity remains in the ceramic regions.

2.1.3 Fabrication of ceramic/polymer architected cellular materials

Hybrid architected materials with a printed topology can be infiltrated with the same process described in Sec. 2.1.2 for a simple coupon. A ceramic truss core sandwich panel is 3D printed entirely in ceramic with the process described in Sec. 2.1.1. After sintering, the bottom face sheet is kept in contact with the resin, which wicked through the face all the way through approximately half the core members. Once the polymer has dried, this process is repeated on the reverse side of the panel. The polymer wicking through the core members will eventually meet the other half of the infiltrated panel and the process stops, resulting in a homogeneous and periodic hybrid cellular material.

2.2 Microstructural characterization

X-ray diffraction (XRD) analysis is conducted on both the starting powder and solid bodies using a Rigaku SmartLab X-ray Diffractometer using Cu-k_α radiation (wavelength 0.15406 nm). Scans consist of 0.05° steps from 20° to 90°. Relative intensity ratio analysis of XRD pattern is used to determined ratio of phases present in sintered bodies. Scanning electron microscopy (SEM) of powders and polished sintered cross-sections was performed using a FEI Magellan 400. A thin film of iridium is deposited on the surface using a South Bay Technology IBS/e Ion Beam Sputter Deposition System to prevent electrical charging during SEM analysis. Energy dispersive spectroscopy (EDS) is performed on the powder and the solid bodies (ceramic and hybrids) with an 80mm² detector (Oxford Instruments) to extract elemental information and allow phase recognition at a small scale.

2.3 Mechanical characterization

To characterize the constituent hybrid material properties, selected truss core members were cut from the panels after infiltration and tested in uniaxial compression. As a reference, cylindrical samples of pure epoxy and un-infiltrated sintered ceramic were also tested. All tests were performed with a servo-electric INSTRON 8862 frame, equipped with a FastTrack 8800 controller and a National Instrument SCXI Data Acquisition system. The displacement rate was controlled at 10μm/s for all tests. The load was measured using the frame load cell (range of 100kN); the displacement, δ, was measured by the internal LVDT embedded in the frame actuator. Engineering stress and strain were used throughout, defined as $\sigma = P/A_0$ and $\varepsilon = \delta/L_0$, with A_0 and L_0 the initial cross-sectional area and length of the sample, respectively. The Young's modulus was obtained from the slope of the stress-strain curve upon unloading. For panel-level compression tests, A_0 is taken as the area of the face sheet and L_0 is the core thickness (distance between the face sheets).

3. RESULTS

3.1 Microstructure of 3D printed ceramics and ceramic/polymer hybrids

3.1.1 Initial powder

The initial powder was very poly-dispersed, with particle size varying between ~10μm and 70μm. SEM/EDS analysis revealed larger alumina particles (both spheroidal and sharp), surrounded by smaller silica fragments (Fig. 4a). X-ray diffraction (XRD) analysis confirmed presence of alumina and indicated absence of mullite in the initial powder. As silica is present as an amorphous phase, it does not show any XRD peak (Fig. 4b).

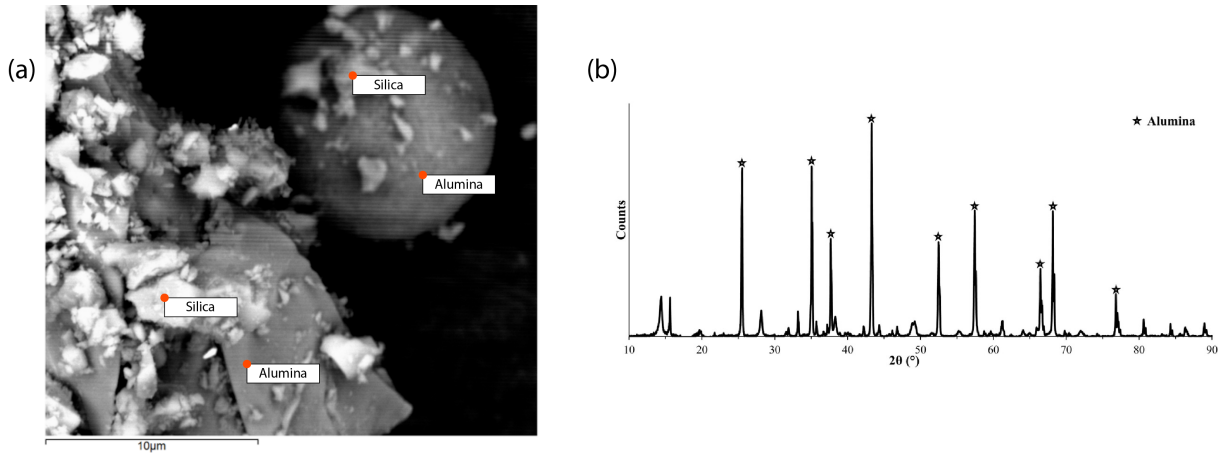

Figure 4 – (a) SEM image of the raw powder, showing alumina and silica particles. (b) XRD spectrum of the powder, revealing only alumina and no mullite (silica is amorphous and hence not showing in the XRD spectrum).

3.1.2 Porous ceramic and dense ceramic/polymer hybrid

Density measurements indicate that the sintered ceramic material has ~50% porosity. The interconnected nature of the porosity (which is essential for the realization of fully dense hybrids) is evident from the micrographs in Fig. 5 (extracted from fracture surfaces of

mechanically compressed cylindrical specimen). The pores are generally ~50 microns in diameter.

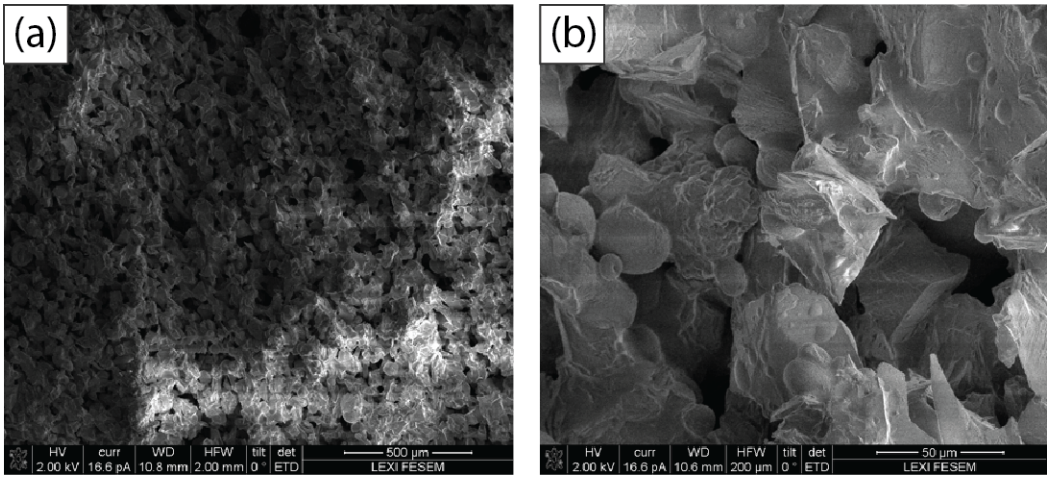

Figure 5 – Fracture surface of the ceramic test coupon. (a) Wide view; (b) Close-up. Notice the extensive interconnected porosity (~50%) and very inhomogeneous microstructure, with small necks connecting large poorly sintered particles. This is consistent with the extremely low strength and modulus reported in Fig. 7.

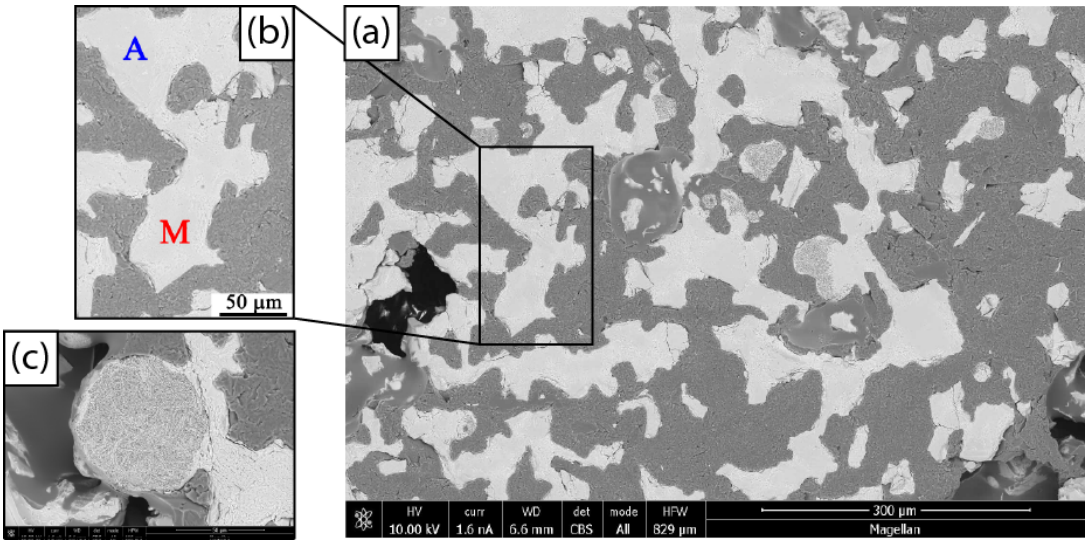

Figure 6 – (a) SEM image of ceramic/polymer hybrid. The dark phase is epoxy. (b) Close-up of the rectangular region in (a), where EDS readings reveal the presence of alumina (A) and mullite (M) phases. (c) Large particles of low-density unsintered alumina are visible.

The microstructure of the fully infiltrated ceramic/epoxy hybrid material (Fig. 6a), approximately showing 50% of ceramic (light phase) and 50% of epoxy (dark phase)

qualitatively confirms the porosity measurements on the ceramic preforms. EDS analyses on a number of ceramic regions reveal both alumina-rich and mullite-rich phases (Fig. 6b), as well as occasional unreacted (not sintered) alumina particles (Fig. 6c). There is no evidence of unreacted silica particles. XRD analysis on the ceramic/epoxy hybrid clearly reveals both alumina and mullite phases, roughly in the ratio 3/1 (estimated from the relative peak intensity, Fig. 7). Once again, amorphous silica is invisible to XRD. If we take the absence of unreacted silica particles as an indication that only alumina and mullite are present, the resulting composition would be 75% alumina – 25% mullite. More extensive characterization is required to fully resolve the quantitative distribution of the phases. Nonetheless, the resulting microstructure is certainly located in the alumina-rich portion of the alumina-silica phase diagram, thus avoiding the mechanical deficiencies associated with segregation of low melting point silica phases at the grain boundaries.

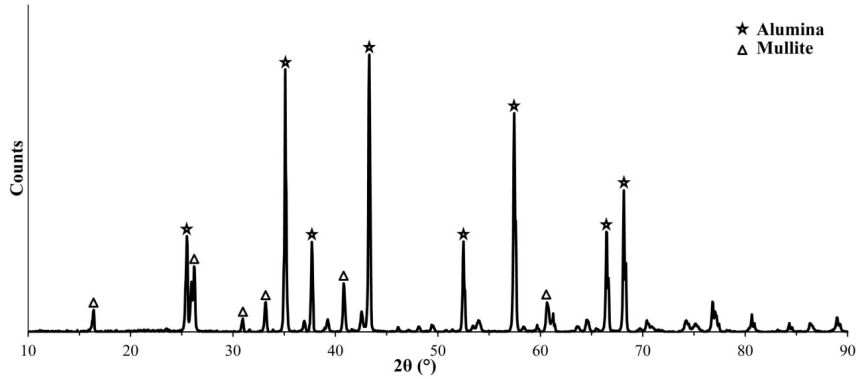

Figure 7 – XRD spectrum of the ceramic/polymer hybrid, revealing both alumina and mullite peaks (silica might be present in amorphous form). Peak ratios indicate that alumina is more prevalent than mullite (in a 3:1 ratio).

3.2 Mechanical performance of ceramic and ceramic/polymer materials

Cylindrical ceramic coupons were printed with the method discussed in Sec. 2.1.1, sintered and tested in uniaxial compression. A representative stress-strain curve is shown in Fig. 8, which also shows the mechanical performance of fully dense epoxy resin. Notice that both the modulus and strength of the porous ceramic are exceptionally low, well below predictions from mechanical foam models. (For foams, $E \sim E_s \overline{\rho}^2$, with E_s the modulus of the parent material and $\overline{\rho}$ the relative density. With $E_s \sim 250$ GPa for 75% alumina / 25% mullite, and $\overline{\rho} \sim 0.5$, we would estimate a modulus for the porous ceramic of ~60 GPa). The significant discrepancy is not surprising, given the morphology of the porous ceramic, essentially consisting of discrete particles loosely connected by sintered ligaments (Fig. 5), unlike the uniform microstructure of foams.

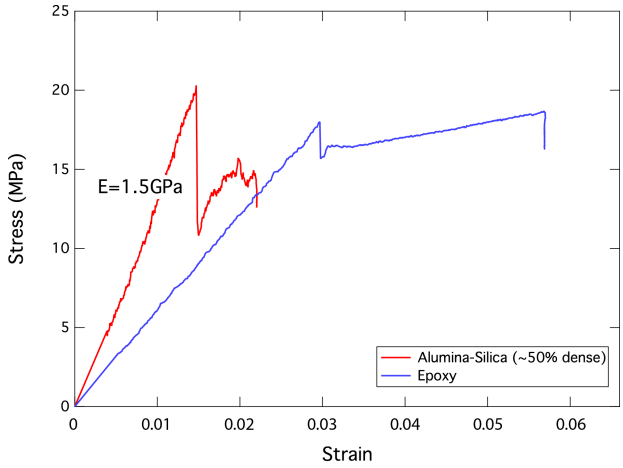

Figure 8 – Compressive response of the sintered printed ceramic material. The material is approximately 50% dense. The mechanical response of the pure epoxy used in subsequent infiltration cycles is reported for comparison.

The compressive response of ceramic/epoxy hybrid test coupons is illustrated in Fig. 9. Fig. 9a shows the stress-strain curves for four different samples, all of which are cut from core members of printed sandwich panels. Two samples (red curves) are nominally identical and have been cut from porous ceramic panels, and subsequently infiltrated in epoxy. The black curves pertain to samples that have been cut from previously infiltrated panels: the solid curve refers to core elements that were at a 45% angle with respect to the face sheets, whereas the dashed curve is for a sample cut from a core member perpendicular to the face sheets (See Fig. 2). A few conclusions emerge: (1) All samples display exceptional strength (~500 MPa, more than 20 times stronger than the porous ceramic) and significant ductility (15-30% strain to failure, versus 1-2% for the porous ceramic). (2) Individually infiltrated samples (red curves) are significantly stiffer (although not necessarily stronger) than samples extracted from previously infiltrated panels (black curves), suggesting that the infiltration procedure for panels (resin is wicked through the face sheets into the core members) is less than 100% effective.

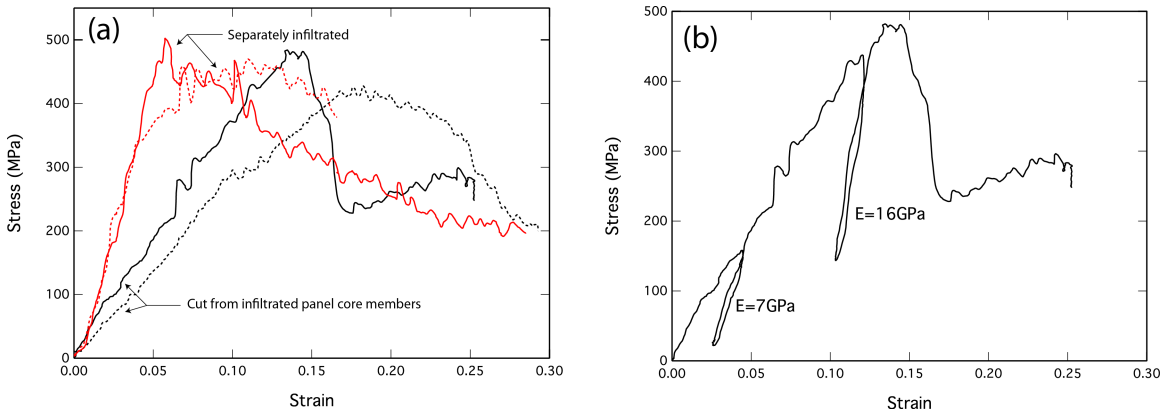

Figure 9 – (a) Compressive response of the fully dense ceramic/epoxy hybrid. (b) Detail from (a), showing unloading/reloading curves for a test coupon cut from a core member of a previously infiltrated sandwich panel. Notice that the modulus increases with straining, likely due to closure of initial residual porosity in the sample.

The most representative stress-strain curve for the core member of infiltrated sandwich panels (solid black curve in Fig. 9a) is reported in Fig. 9b (including unloading/reloading portions) for clarity. Notice the stiffening effect induced by compressive straining. This is again consistent with the presence of some small amount of initial porosity, which is progressively filled upon loading.

3.3 Mechanical performance of hybrid truss-core sandwich panels

The compressive response of truss-core sandwich panels with hybrid (ceramic/epoxy) constituent material (fabricated as described in Sec. 2.1.3) is shown in Fig. 10. The core exhibits a fairly brittle behavior, with an effective strength of ~7 MPa. The sharp stress drops on the loading portion of the stress-strain curve are likely associated with shear failure at the truss/face sheet interface. This is consistent with the unexpectedly low effective strength of the panel. Basic mechanics models predict an effective strength $\sigma_c = \pi(D/L)^2\sigma_c^0/\sqrt{2}$, where D and L are the diameter and the length of the truss member, respectively, the core members are at 45^0 from the horizontal plane and σ_c^0 is the compressive strength of the constituent material. With D~2mm, L~15mm and $\sigma_c^0 \sim 450$ MPa, the effective strength of the core is expected to be ~26 MPa, almost 4 times higher than the experimental measurement. The conclusion is that the weak response of the nodes under shear loads must be addressed: switching to a dip coating process whereby the whole panel is submerged in resin, rather than wicking from the outside, will likely significantly improve the microstructure at the nodes and hence the mechanical properties of the panel.

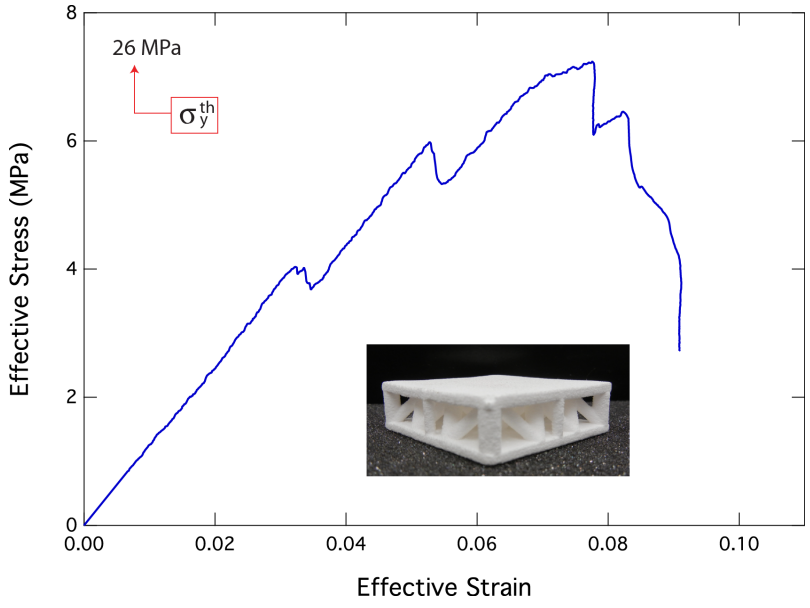

Figure 10 – Compressive response of a printed, sintered and infiltrated hybrid sandwich panel. Based on the constituent material response in Fig. 9b, basic mechanics predict a panel strength of ~26 MPa. Shear failure at the nodes is responsible for the premature collapse of the panel.

4. CONCLUSIONS

This work demonstrated a novel additive manufacturing approach for architected materials and structures comprising ceramic or ceramic/polymer hybrid structural elements. The architected material is 3D printed in ceramic powder (alumina/silica) in its final shape and subsequently sintered, resulting in an alumina/mullite architected material. The processing parameters were adjusted to result in a porous alumina/mullite microstructure, allowing filling the interconnected porosity with a low curing epoxy resin. The result is an architected material where the constituent material is a fully dense alumina/mullite/epoxy hybrid. The mechanical performance of this hybrid constituent material under compression was characterized: the material exhibits strength in excess of 500MPa and strain to failure as high as 30%. The resulting architected material (in the form of a truss-core sandwich panel) loaded in compression underperformed relative to the base material strength, indicating that the low shear strength of the nodes is a weak link in the microstructure. Future work will address superior node design and the manufacturing and characterization of functionally graded hybrid architected materials.

5. REFERENCES

[1] A. K. Noor, Ed., *Structures Technology for Future Aerospace Systems*, vol. 188. AIAA.

[2] T. Lu, L. Valdevit, and A. Evans, "Active cooling by metallic sandwich structures with periodic cores," *Prog Mater Sci*, vol. 50, no. 7, pp. 789–815, 2005.

[3] L. Valdevit, J. Hutchinson, and A. Evans, "Structurally optimized sandwich panels with prismatic cores," *Int J Solids Struct*, vol. 41, no. 18, pp. 5105–5124, 2004.

[4] L. Valdevit, A. Pantano, H. Stone, and A. Evans, "Optimal active cooling performance of metallic sandwich panels with prismatic cores," *International Journal of Heat and Mass Transfer*, vol. 49, no. 21, pp. 3819–3830, 2006.

[5] F. Zok, S. Waltner, Z. Wei, H. Rathbun, R. McMeeking, and A. Evans, "A protocol for characterizing the structural performance of metallic sandwich panels: application to pyramidal truss cores," *Int J Solids Struct*, vol. 41, no. 22, pp. 6249–6271, 2004.

[6] L. Valdevit, A. J. Jacobsen, J. R. Greer, and W. B. Carter, "Protocols for the Optimal Design of Multi-Functional Cellular Structures: From Hypersonics to Micro-Architected Materials," *Journal of the American Ceramic Society*, vol. 94, pp. 15–34, Jun. 2011.

[7] L. Valdevit, N. Vermaak, F. Zok, and A. Evans, "A Materials Selection Protocol for Lightweight Actively Cooled Panels," *Journal of Applied Mechanics*, vol. 75, p. 061022, 2008.

[8] N. Vermaak, L. Valdevit, and A. Evans, "Materials Property Profiles for Actively Cooled Panels: An Illustration for Scramjet Applications," *Metallurgical and Materials Transactions A*, vol. 40, no. 4, pp. 877–890, 2009.

[9] N. Vermaak, L. Valdevit, A. G. Evans, F. W. Zok, and R. M. McMeeking, "Implications of shakedown for design of actively cooled thermostructural panels," *J Mech Mater Struct*, vol. 6, no. 9, pp. 1313–1327, Jan. 2012.